Coupled Thermal and Power Transport of Optical Waveguide Arrays: Photonic Wiedemann-Franz Law and Rectification Effect

Meng Lian,[1] Yue Geng,[1] Yin-Jie Chen,[1] Yuntian Chen,[2,3] and Jing-Tao Lü[1,*]

[1]School of Physics, Institute for Quantum Science and Engineering and Wuhan National High Magnetic Field Center, Huazhong University of Science and Technology, Wuhan 430074, China

[2]School of Optical and Electronic Information, Huazhong University of Science and Technology, Wuhan 430074, China

[3]Wuhan National Laboratory for Optoelectronics, Huazhong University of Science and Technology, Wuhan 430074, China

(Received 17 August 2023; revised 27 May 2024; accepted 31 July 2024; published 11 September 2024)

In isolated nonlinear optical waveguide arrays, simultaneous conservation of longitudinal momentum flow ("internal energy") and optical power ("particle number") of the optical modes enables study of coupled thermal and particle transport in the negative temperature regime. Based on exact numerical simulation and rationale from Landauer formalism, we predict generic photonic version of the Wiedemann-Franz law in such systems, with the Lorenz number $L \propto |T|^{-2}$. This is rooted in the spectral decoupling of thermal and particle current, and their different temperature dependence. In addition, in asymmetric junctions, relaxation of the system toward equilibrium shows apparent asymmetry for positive and negative biases, indicating rectification behavior. This Letter illustrates the possibility of simulate nonequilibrium transport processes using optical networks, in parameter regimes difficult to reach in natural condensed matter or atomic gas systems. It also provides new insights in manipulating power and momentum flow of optical waves in artificial waveguide arrays.

DOI: 10.1103/PhysRevLett.133.116303

Precisely engineered optical systems have enabled study of problems originated from condensed matter and other branches of physics in clean and controllable setups [1–3]. Recently, such effort has been extended from linear, Hermitian to nonlinear, non-Hermitian systems [4–8]. An important insight is description of the complex behavior of weakly nonlinear coupled optical waveguide arrays within the framework of statistical thermodynamics [9–11]. It provides fresh new insight in understanding puzzling optical phenomena, such as beam self-cleaning [12–14], spatiotemporal solitons [15–17], mode-locking [18], from the point of view of statistical mechanics [19–25].

Given simultaneous particle and energy conservation, relaxation of an initially nonequilibrium state toward equilibrium is frequently accompanied by particle and thermal transport mediated by nonlinear interactions within the system. As a cornerstone result of linear irreversible thermodynamics [26], such coupled transport of particle and thermal current is characterized by a transport matrix, whose diagonal and off-diagonal elements correspond to particle (G), thermal (G_T) conductance (conductivity), and thermoparticle (Seebeck and Peltier) transport coefficients, respectively. Study of these transport properties has gained invaluable information on the equilibrium and nonequilibrium properties of condensed matter and atomic gases [27–36]. The celebrated Wiedemann-Franz (W-F) law links particle and thermal transport coefficients of the system. It is characterized by the Lorenz number $L = G_T/(GT)$, which is constant in Fermi liquids $L_0 = k_B^2\pi^2/3$ with k_B the Boltzmann constant. Deviation from the W-F law indicates decoupling of particle and thermal transport [36,37], whose origin ranges from strong interparticle interaction to singular quasiparticle density of states. Thus, L has become an important parameter in the study of wide range of problems, including thermoelectric [38,39], hydrodynamic [40,41], strong correlated effects [42], to name a few.

In weakly nonlinear waveguide arrays, the total optical power and the longitudinal momentum flow along the waveguides are two conserved quantities. In optical thermodynamic theory, they are considered as particle number and internal energy, respectively. This curious correspondence makes it possible to study coupled particle and thermal transport in transport junctions made from such optical systems, which is difficult in natural condensed matter system with phonons or magnons due to the lack of quasiparticle number conservation. By numerically tracking the thermalization process, we predict a generic photonic version of the W-F law in such junctions, with the Lorenz number $L \propto 1/T^2$ [see Fig. 1(a)]. It does not depend on details of the lattice structure, model parameters, and is valid in both positive and negative temperature regimes. We provide a rationale of this result using the Landauer transport theory in the classical limit. Furthermore, we observe asymmetric relaxation of a

*Contact author: jtlu@hust.edu.cn

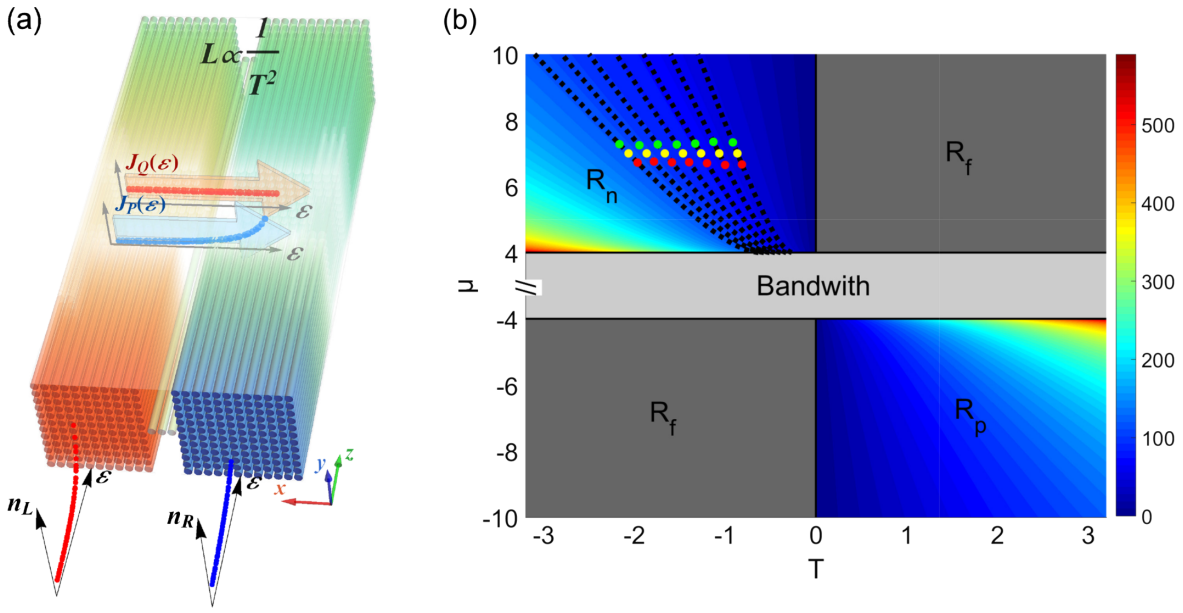

FIG. 1. (a) Transport junction made from nonlinear waveguide arrays with square reservoirs. The one-dimensional chain bridges the left and right reservoirs, such that particle and thermal transport between them can take place. The system is initialized at lower end of the waveguides, where the two reservoirs are at their own equilibrium state, characterized by equilibrium Rayleigh-Jeans distribution n_L and n_R. The initial condition can be realized by elongating the waveguides that belong to the two reservoirs without the central chain, such that the input power and internal energy in each reservoir can relax separately. Once the central chain is introduced, the whole junction relaxes toward equilibrium while propagating along z direction. A generic photonic Wiedemann-Franz law is predicted with the Lorenz number $L \propto T^{-2}$, indicating decoupled thermal (J_Q) and power (J_P) current. Shown in the inset is the energy dependence of $J_Q(\varepsilon)$ and $J_P(\varepsilon)$ for constant transmission $\mathcal{T}$. (b) (T, μ) phase diagram of the square reservoir. R_{p} and R_{n} represent the positive and negative temperature regime, respectively. No equilibrium state exists in the R_{f} regime. Power (P) for given (T, μ) is represented by the colored code. The black dashed lines are the isopower lines. The red (green) dots are the initial parameters of the left (right) reservoir, while the yellow dots are their average $\bar{T}$ and $\bar{\mu}$.

junction connecting a square and a honeycomb reservoir with different sizes, indicating rectification behavior in asymmetric junctions in the presence of nonlinear interaction. This Letter illustrates the opportunity to study fundamental problems of statistical thermodynamics in unprecedented regimes using engineered optical systems [43–45]. It may help to resolve the debate on the legitimacy of negative absolute temperature in thermodynamics [46,47].

Model—We consider transport junction made from two-dimensional waveguide arrays, which consists of two large but finite-size reservoirs connected by a chain. We study coupled thermal and power transport properties across the chain. As shown in Fig. 1(a), each node represents a waveguide, along which (z direction) the optical wave can propagate. In the reservoir the nodes are periodically arranged. This is a prototypical junction structure to study transport properties of solid-state [48] and cold atom systems [49].

Propagation of the optical modes along the waveguides is described by the discrete nonlinear Schrödinger equation [50,51],

$$i\frac{d\psi_m}{dz} + \kappa\sum_{\{n\}}\psi_n + \chi|\psi_m|^2\psi_m = 0, \tag{1}$$

with dimensionless parameters ψ_m, κ, χ representing the complex wave amplitude, the nearest neighbor coupling between waveguides and Kerr-type nonlinear coefficient, respectively. Here, the coordinate z along waveguide plays the role of time in standard Schrödinger equation, and $\{n\}$ includes all the nearest neighbors of m.

For weak nonlinear interactions, we can diagonalize the linear term and obtain the corresponding eigenmode (supermode) propagating constant β_k and corresponding vector φ_k. For a given state ψ, the modal occupancy is obtained by projection onto each supermode $|c_k|^2 = |\langle\varphi_k|\psi\rangle|^2$. The system evolves with conserved internal energy $U = \sum_{k=1}^{M}\varepsilon_k|c_k|^2$ and optical power $P = \sum_{k=1}^{M}|c_k|^2$, with the total number of modes M, the eigen energy defined by the negative of β_k as $\varepsilon_k = -\beta_k$ with $\beta_1 \geq \beta_2 \geq \cdots \geq \beta_M$. The system thus has a bounded spectrum between $[\varepsilon_1, \varepsilon_M]$. The weak nonlinear part introduces coupling among different supermodes, such that the system can thermalize to an equilibrium state through energy and power redistribution among supermodes. It plays a role similar to molecular collisions in ideal gas.

Equilibrium thermodynamic theory—We can use the optical thermodynamic theory to describe each reservoir [9] (details in Sec. I of the Supplemental Material

(SM) [52]). For each reservoir (omitting reservoir index), starting from the optical entropy,

$$S = \sum_{k=1}^{M} \ln |c_k|^2, \tag{2}$$

using the maximum entropy principle, the mode occupancy can be obtained, which follows the classical Rayleigh-Jeans (R-J) distribution at thermal equilibrium,

$$n(\varepsilon_k) = |c_k|^2 = \frac{T}{\varepsilon_k - \mu}. \tag{3}$$

Here, T is the dimensionless optical temperature, μ is the optical chemical potential. The reservoir internal energy can be written as

$$U = MT + \mu P. \tag{4}$$

One prominent feature we can find is that, for given power P, the optical entropy S no longer varies monotonically with the internal energy U. Consequently, the system can reach the negative optical temperature regime [9,58]. From Eqs. (3), (4), we have plotted the phase diagram of the reservoir with square lattice. As shown in Fig. 1(b), only $\{(T,\mu)|T<0,\mu>\varepsilon_M\}$ (R_n) and $\{(T,\mu)|T>0,\mu<\varepsilon_1\}$ (R_p) can be visited, and the other regimes are forbidden (R_f). This follows from the requirement $|c_k|^2 \geq 0$. Moreover, the chemical potential is out of the band spectrum of the system, i.e., μ is below (above) the lowest (highest) energy level for positive (negative) temperature. The positive and negative temperature regimes are antisymmetric with each other in the phase diagram when neglecting the nonlinear effect. In the following, we focus on the negative temperature regime and numerically check that this antisymmetry is still approximately valid in the weakly nonlinear regime (Fig. 2).

Transport coefficients in microcanonical ensemble—Transport theory is normally formulated with open boundaries using grand canonical ensemble. Current is driven by temperature or chemical potential bias between two reservoirs of infinite size. Because of finite size of present junction, it is convenient to utilize the microcanonical setup. The transport coefficients can be extracted by following the thermalization process of a microcanonical system from given initial conditions, where the left and right reservoirs are at their own thermodynamic equilibrium with different chemical potential or temperature.

Using the theory of irreversible thermodynamics, we can make connection between chemical potential ($\Delta\mu$) and temperature (ΔT) biases (affinities) with the corresponding power (J_P) and entropy (J_S) currents (fluxes). The corresponding transport matrix connecting affinities and fluxes follows the Onsager symmetry

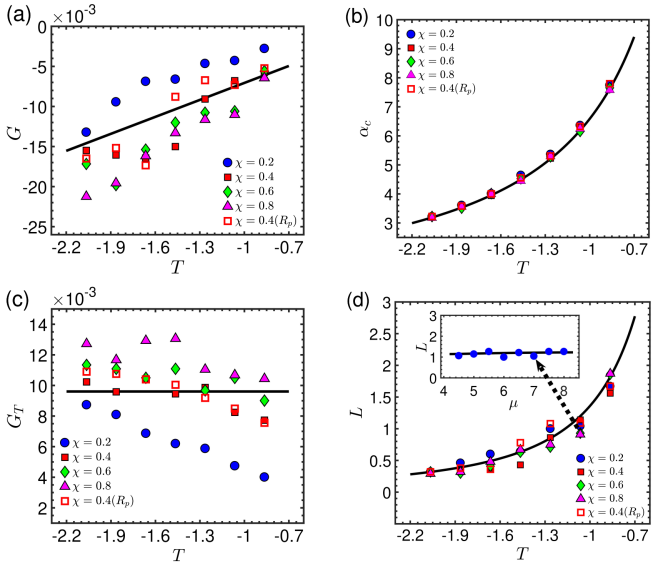

FIG. 2. Dependence of transport coefficients on temperature (T) for different nonlinear strengths χ at $\bar{\mu} = 7$ for the structure shown in Fig. 1(a) with $\kappa = 1$, $M = 19 \times 19$. Convergence of the results with respect to reservoir size M is given in Sec. II-C of the SM. (a) Conductance G, (b) Seebeck coefficient α_c, (c) thermal conductance G_T, (d) Lorenz number L. The inset shows dependence of L on chemical potential μ at $T = -1.06$ and $\chi = 0.2$. The black solid lines are theoretical results from the Landauer formalism. Results at positive temperature with $\chi = 0.4$ are shown with empty squares. The sign of T and G at positive T are reversed to show in the figure. They are very close to those at corresponding negative temperature (filled squares).

$$\begin{pmatrix} J_P \\ J_S \end{pmatrix} = \begin{pmatrix} K_0 & K_1/T \\ K_1/T & K_2/T^2 \end{pmatrix} \begin{pmatrix} \Delta\mu \\ \Delta T \end{pmatrix}. \tag{5}$$

Here, $J_P = -(\partial \Delta P/\partial z)/2$, $J_S = -(\partial \Delta S/\partial z)/2$, and $\Delta P = P_L - P_R$; $\Delta S = S_L - S_R$ represent difference between the macroscopic quantities of the left and right reservoirs. Positive direction of the currents is chosen as from left to right. The matrix elements K_0, K_1, and K_2 depend on the structure of the chain and the state of the whole system. We can obtain the evolution equations of ΔP and ΔT by eliminating $\Delta\mu$ and ΔS using the equilibrium thermodynamic relations of the two reservoirs (see Sec. II of SM for details [52]). For symmetric junctions with identical left and right reservoirs, they read

$$\tau_0 \frac{\partial}{\partial z} \begin{pmatrix} \Delta P \\ \Delta T \end{pmatrix} = -\begin{pmatrix} 1 & -\kappa\alpha \\ -\frac{\alpha}{l\kappa} & \frac{L+\alpha^2}{l} \end{pmatrix} \begin{pmatrix} \Delta P \\ \Delta T \end{pmatrix}, \tag{6}$$

where we have defined a transport timescale $\tau_0 = \kappa/(2G)$. The reservoir properties κ, α_r, C_P are the compression coefficient, Seebeck coefficient, and the heat capacity at constant power, respectively, with $l = C_P/T\kappa$. They are evaluated at the average temperature and chemical potential [Eqs. (S33)–(S35)]. The effective Seebeck coefficient

$\alpha = \alpha_r - \alpha_c$ characterizes the difference between the reservoir itself α_r and the whole junction α_c.

General solutions of the above equations are

$$\Delta P(z) = \left(\frac{\Omega+\delta-1}{2\Omega}\Delta P_0 + \frac{\alpha\kappa}{2\Omega}\Delta T_0\right) \times e^{-\frac{z}{\tau_>}}\left[1+\frac{(\Omega-\delta+1)\Delta P_0 - \alpha\kappa\Delta T_0}{(\Omega+\delta-1)\Delta P_0 + \alpha\kappa\Delta T_0}e^{-\frac{z}{\tau_<}}\right], \quad (7)$$

$$\Delta T(z) = \left(\frac{\Omega-\delta+1}{2\Omega}\Delta T_0 + \frac{\alpha}{2l\kappa\Omega}\Delta P_0\right) \times e^{-\frac{z}{\tau_>}}\left[1+\frac{l\kappa(\Omega+\delta-1)\Delta T_0 - \alpha\Delta P_0}{l\kappa(\Omega-\delta+1)\Delta T_0 + \alpha\Delta P_0}e^{-\frac{z}{\tau_<}}\right], \quad (8)$$

where $\delta = [1 + (L + \alpha^2)/l]/2$ and $\Omega = \sqrt{\delta^2 - L/l}$ form the eigenvalues of the evolutionary matrix $\lambda_\pm = \delta \pm \Omega$. The fast and slow timescales $\tau_< = \tau_0/2\Omega$ and $\tau_> = \tau_0/(\delta - \Omega)$ indicate the evolution of the system in two stages (Fig. S3): (1) a saturation process is characterized by the timescale $\tau_<$, which dominates the initial short time period. This process leads to an initial increase in the absolute value of the particle number deviation until it reaches a maximum. (2) A decay process is characterized by the timescale $\tau_>$, which dominates the longer period of time after saturation. The three transport coefficients G, α_c, and L (or G_T) can then be acquired by fitting the numerical results obtained from solving the discrete nonlinear Schrödinger equation. Details of the fitting procedure can be found in Sec. II-B of the SM [52].

Photonic Wiedemann-Franz law—Figure 2 shows temperature dependence of the transport coefficients for a symmetric junction with square-lattice reservoirs. We notice that, in the negative temperature regime, conductance $G < 0$, indicating that the power is transferred from the low to the high chemical potential reservoir when $\Delta T = 0$. This seemingly surprising result does not violate the second law of thermodynamics. Considering two subsystems that can exchange particles with each other under constant temperature, the second law of thermodynamics requires that the entropy does not decrease during the particle exchange $\Delta S = (\mu_L - \mu_R)\Delta P/T > 0$, where ΔP is the power lost from the left reservoir or gained from the right reservoir. When $T > 0$, the power is transferred from high to low chemical potential. However, in the opposite case of $T < 0$, the direction is reversed, meaning $G < 0$. Similar argument applies to the case of thermal transport in the presence of temperature bias $\Delta S = -({T_L}^{-1} - {T_R}^{-1})\Delta Q > 0$, with ΔQ heat transferred out of the left reservoir. This indicates that the direction of thermal current is from high to low temperature, thus $G_T > 0$.

Figure 2(a) shows an approximated linear T dependence of G for all the nonlinear parameters considered. This can be understood qualitatively from the Landauer formalism (Sec. III of SM [52]).

The conductance can be approximated as

$$G = \int \frac{d\varepsilon}{2\pi}\mathcal{T}(\varepsilon)\frac{T}{(\varepsilon-\mu)^2}, \quad (9)$$

indicating $G \propto T$ for temperature independent transmission $\mathcal{T}(\varepsilon)$. Moreover, the optical modes contribute to the transport with a weighting factor inversely proportional to the square of the energy deviation from the chemical potential.

Temperature dependence of the Seebeck coefficient α_c is shown in Fig. 2(b). It can be well fitted by an inverse T dependence $\alpha_c \propto -1/T$ predicted by the Landauer model. The little effect of nonlinear interaction on α_c can also be captured by the Landauer result. In fact, α_c can be written as $\alpha_c = K_1/(K_0 T)$. K_0 and K_1 have similar dependence on the nonlinear interaction, they cancel with each other in α_c.

Similar to conductance, the thermal conductance G_T also increases with nonlinearity [Fig. 2(c)]. From the Landauer formalism, we get

$$G_T = \int \frac{d\varepsilon}{2\pi}\mathcal{T}(\varepsilon) - T\alpha_c^2 G. \quad (10)$$

This gives a temperature independent G_T. Similar to G, the temperature dependence in the numerical results is due to nonlinear interaction. The second term on the right side of Eq. (10) represents correction to the thermal conductance due to Seebeck coefficient. Here, its magnitude is comparable to the first term. This is in contrast to the case of electrons in condensed matter system, where the thermoelectric correction is often negligible.

The variation of L with temperature and chemical potential is shown in Fig. 2(d), and is once again captured by Landauer's theory. It can be found that the Lorenz number is more sensitive to temperature than the chemical potential (inset). In the Landauer picture, $G_T \propto T^0$ together with $G \propto T$ leads to $L \propto 1/T^2$, which is the photonic W-F law. The decrease in L with decreasing temperature comes from the increase in $|G|$. Similar to α_c, we also observe a rather weak dependence on the strength of nonlinear interaction. Thus, the $|T|^{-2}$ dependence of the Lorenz number is not due to nonlinear interaction. Rather, its origin is similar to that in coherent mescoscopic conductors, which can be fully accounted by the single particle Landauer formalism. Similar results are obtained for reservoirs with honeycomb lattices (SM, Sec. IV [52]).

Rectification in an asymmetric junction—While the transport coefficients are well-defined only in the linear regime, the numerical solution of Eq. (1) applies equally in nonequilibrium situation. Figure 3 depicts results obtained for an asymmetric junction with square and honeycomb reservoirs at left and right, respectively [Fig. 3(c), inset]; see also Sec. V of SM [52]. We have applied initial chemical potential ($|\Delta\mu| = 10$) or temperature ($|\Delta T| = 5$)

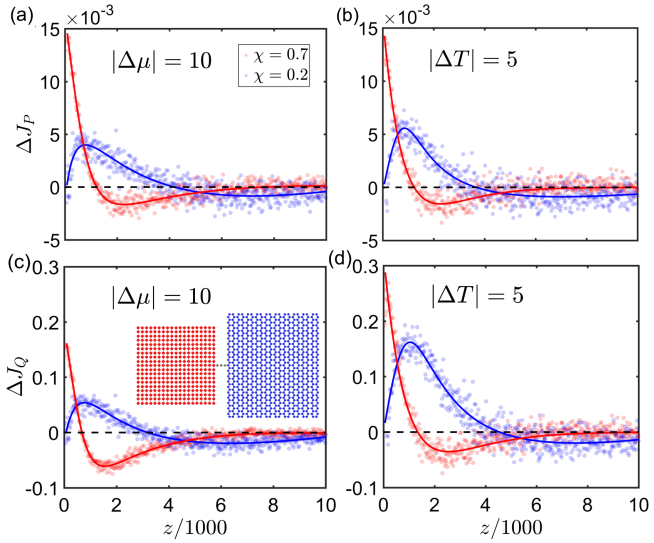

FIG. 3. Difference in the power [$\Delta J_P = J_P^+ - J_P^-$, (a),(b)] and thermal [$\Delta J_Q = J_Q^+ - J_Q^-$, (c),(d)] current for positive and negative bias in chemical potential [$|\Delta\mu| = 10$, (a),(c)] and temperature [$|\Delta T| = 5$, (b),(d)] (see also Fig. S8). Schematic of the asymmetric junction is shown in the inset of (c). The dots are the numerical data and the lines are guides to the eye. The square reservoir has a size $M = 19 \times 19$ and nearest neighbor coupling $\kappa = 1$, while the honeycomb reservoir has $M = 20 \times 39$, $\kappa = 2$. Positive bias is defined as $\mu_L > \mu_R$, $T_L > T_R$.

bias beyond linear regime. The difference in power and thermal current at positive and negative bias $(\Delta J_P, \Delta J_Q)$ during relaxation is shown for nonlinear coefficients $\chi = 0.7$ (red) and 0.2 (blue). The different behavior for the two bias direction indicates rectification effect in both power and thermal current, which grows with increasing χ. For $\chi = 0.2$, the current difference grows to a maximum and decays slowly afterward. It takes longer time for the nonlinear effect to build up and for the system to relax to equilibrium, compared to the case of $\chi = 0.7$. The overall results are consistent with the general theory, which predicts rectification behavior in asymmetric junction with nonlinear interactions [59–62]. The maximum rectification ratio (defined as current difference over average) is ~30%, consistent with result from simulation using grand canonical ensemble at steady state using Langevin baths [63]. In Fig. 3, both lattice type and reservoir size are different. We have checked that rectification can still be observed when there is only one type of asymmetry, although the magnitude changes (Sec. V of SM [52]).

In conclusion, based on a theory in the microcanonical ensemble, we found a photonic Wiedemann-Franz law, with the Lorenz number $L \propto 1/T^2$, in coupled optical power and thermal transport of nonlinear waveguide arrays. Moreover, asymmetric relaxation behavior is found in a junction with square and honeycomb lattices, indicating rectification behavior in both power and thermal transport. Our findings are of great importance for the study of fundamental nonequilibrium thermodynamic processes utilizing artificial optical waveguide arrays, where coupled power and thermal transport is ubiquitous. Moreover, since the internal energy represents longitudinal momentum flow of optical modes in the waveguides, it would be interesting to explore these theoretical results in designing novel devices to manipulate optical waves. Estimation of the parameters in realistic optical systems is given in Sec. VI of SM [52].

Note added—During the submission of this work, we became aware of a related work [64], where a similar relation between G_T and G is derived.

Acknowledgments—This work was supported by the National Key Research and Development Program of China (Grant No. 2022YFA1402400) and the National Natural Science Foundation of China (Grant No. 22273029).

[1] E. Yablonovitch, Inhibited spontaneous emission in solid-state physics and electronics, Phys. Rev. Lett. **58**, 2059 (1987).
[2] S. John, Strong localization of photons in certain disordered dielectric superlattices, Phys. Rev. Lett. **58**, 2486 (1987).
[3] F. D. M. Haldane and S. Raghu, Possible realization of directional optical waveguides in photonic crystals with broken time-reversal symmetry, Phys. Rev. Lett. **100**, 013904 (2008).
[4] M.-A. Miri and A. Alù, Exceptional points in optics and photonics, Science **363**, eaar7709 (2019).
[5] R. El-Ganainy, K. G. Makris, M. Khajavikhan, Z. H. Musslimani, S. Rotter, and D. N. Christodoulides, Non-Hermitian physics and PT symmetry, Nat. Phys. **14**, 11 (2018).
[6] L. G. Wright, F. O. Wu, D. N. Christodoulides, and F. W. Wise, Physics of highly multimode nonlinear optical systems, Nat. Phys. **18**, 1018 (2022).
[7] A. Fusaro, J. Garnier, K. Krupa, G. Millot, and A. Picozzi, Dramatic acceleration of wave condensation mediated by disorder in multimode fibers, Phys. Rev. Lett. **122**, 123902 (2019).
[8] N. Berti, K. Baudin, A. Fusaro, G. Millot, A. Picozzi, and J. Garnier, Interplay of thermalization and strong disorder: Wave turbulence theory, numerical simulations, and experiments in multimode optical fibers, Phys. Rev. Lett. **129**, 063901 (2022).
[9] F. O. Wu, A. U. Hassan, and D. N. Christodoulides, Thermodynamic theory of highly multimoded nonlinear optical systems, Nat. Photonics **13**, 776 (2019).
[10] M. Parto, F. O. Wu, P. S. Jung, K. Makris, and D. N. Christodoulides, Thermodynamic conditions governing the optical temperature and chemical potential in nonlinear highly multimoded photonic systems, Opt. Lett. **44**, 3936 (2019).
[11] K. G. Makris, F. O. Wu, P. S. Jung, and D. N. Christodoulides, Statistical mechanics of weakly nonlinear optical multimode gases, Opt. Lett. **45**, 1651 (2020).

[12] K. Krupa, A. Tonello, B. M. Shalaby, M. Fabert, A. Barthélémy, G. Millot, S. Wabnitz, and V. Couderc, Spatial beam self-cleaning in multimode fibres, Nat. Photonics **11**, 237 (2017).
[13] Z. Liu, L. G. Wright, D. N. Christodoulides, and F. W. Wise, Kerr self-cleaning of femtosecond-pulsed beams in graded-index multimode fiber, Opt. Lett. **41**, 3675 (2016).
[14] A. Niang, T. Mansuryan, K. Krupa, A. Tonello, M. Fabert, P. Leproux, D. Modotto, O. N. Egorova, A. E. Levchenko, D. S. Lipatov, S. L. Semjonov, G. Millot, V. Couderc, and S. Wabnitz, Spatial beam self-cleaning and supercontinuum generation with Yb-doped multimode graded-index fiber taper based on accelerating self-imaging and dissipative landscape, Opt. Express **27**, 24018 (2019).
[15] T. Herr, V. Brasch, J. D. Jost, C. Y. Wang, N. M. Kondratiev, M. L. Gorodetsky, and T. J. Kippenberg, Temporal solitons in optical microresonators, Nat. Photonics **8**, 145 (2014).
[16] L. G. Wright, D. N. Christodoulides, and F. W. Wise, Controllable spatiotemporal nonlinear effects in multimode fibres, Nat. Photonics **9**, 306 (2015).
[17] V. L. Kalashnikov and S. Wabnitz, Stabilization of spatio-temporal dissipative solitons in multimode fiber lasers by external phase modulation, Laser Phys. Lett. **19**, 105101 (2022).
[18] L. G. Wright, D. N. Christodoulides, and F. W. Wise, Spatiotemporal mode-locking in multimode fiber lasers, Science **358**, 94 (2017).
[19] P. S. Jung, G. G. Pyrialakos, F. O. Wu, M. Parto, M. Khajavikhan, W. Krolikowski, and D. N. Christodoulides, Thermal control of the topological edge flow in nonlinear photonic lattices, Nat. Commun. **13**, 4393 (2022).
[20] G. G. Pyrialakos, H. Ren, P. S. Jung, M. Khajavikhan, and D. N. Christodoulides, Thermalization dynamics of nonlinear non-Hermitian optical lattices, Phys. Rev. Lett. **128**, 213901 (2022).
[21] C. Shi, T. Kottos, and B. Shapiro, Controlling optical beam thermalization via band-gap engineering, Phys. Rev. Res. **3**, 033219 (2021).
[22] D. Leykam, E. Smolina, A. Maluckov, S. Flach, and D. A. Smirnova, Probing band topology using modulational instability, Phys. Rev. Lett. **126**, 073901 (2021).
[23] J. Bloch, I. Carusotto, and M. Wouters, Non-equilibrium Bose–Einstein condensation in photonic systems, Nat. Rev. Phys. **4**, 470 (2022).
[24] Z. Xiong, F. O. Wu, J.-T. Lü, Z. Ruan, D. N. Christodoulides, and Y. Chen, *k*-space thermodynamic funneling of light via heat exchange, Phys. Rev. A **105**, 033529 (2022).
[25] K. Baudin, A. Fusaro, K. Krupa, J. Garnier, S. Rica, G. Millot, and A. Picozzi, Classical Rayleigh-Jeans condensation of light waves: Observation and thermodynamic characterization, Phys. Rev. Lett. **125**, 244101 (2020).
[26] H. B. Callen and T. A. Welton, Irreversibility and generalized noise, Phys. Rev. **83**, 34 (1951).
[27] J.-P. Brantut, C. Grenier, J. Meineke, D. Stadler, S. Krinner, C. Kollath, T. Esslinger, and A. Georges, A thermoelectric heat engine with ultracold atoms, Science **342**, 713 (2013).
[28] C. Nietner, G. Schaller, and T. Brandes, Transport with ultracold atoms at constant density, Phys. Rev. A **89**, 013605 (2014).
[29] F. Gallego-Marcos, G. Platero, C. Nietner, G. Schaller, and T. Brandes, Nonequilibrium relaxation transport of ultracold atoms, Phys. Rev. A **90**, 033614 (2014).
[30] S. Häusler, P. Fabritius, J. Mohan, M. Lebrat, L. Corman, and T. Esslinger, Interaction-assisted reversal of thermopower with ultracold atoms, Phys. Rev. X **11**, 021034 (2021).
[31] E. L. Hazlett, L.-C. Ha, and C. Chin, Anomalous thermoelectric transport in two-dimensional Bose gas, arXiv:1306.4018.
[32] D. J. Papoular, L. P. Pitaevskii, and S. Stringari, Fast thermalization and Helmholtz oscillations of an ultracold Bose gas, Phys. Rev. Lett. **113**, 170601 (2014).
[33] A. Rançon, C. Chin, and K. Levin, Bosonic thermoelectric transport and breakdown of universality, New J. Phys. **16**, 113072 (2014).
[34] S. Uchino and J.-P. Brantut, Bosonic superfluid transport in a quantum point contact, Phys. Rev. Res. **2**, 023284 (2020).
[35] D. Husmann, S. Uchino, S. Krinner, M. Lebrat, T. Giamarchi, T. Esslinger, and J.-P. Brantut, Connecting strongly correlated superfluids by a quantum point contact, Science **350**, 1498 (2015).
[36] D. Husmann, M. Lebrat, S. Häusler, J.-P. Brantut, L. Corman, and T. Esslinger, Breakdown of the Wiedemann-Franz law in a unitary Fermi gas, Proc. Natl. Acad. Sci. U.S.A. **115**, 8563 (2018).
[37] S. Lee, K. Hippalgaonkar, F. Yang, J. Hong, C. Ko, J. Suh, K. Liu, K. Wang, J. J. Urban, X. Zhang, C. Dames, S. A. Hartnoll, O. Delaire, and J. Wu, Anomalously low electronic thermal conductivity in metallic vanadium dioxide, Science **355**, 371 (2017).
[38] B. Kubala, J. König, and J. Pekola, Violation of the Wiedemann-Franz law in a single-electron transistor, Phys. Rev. Lett. **100**, 066801 (2008).
[39] I. Kostylev, A. A. Zadorozhko, M. Hatifi, and D. Konstantinov, Thermoelectric transport in a correlated electron system on the surface of liquid helium, Phys. Rev. Lett. **127**, 186801 (2021).
[40] J. Crossno, J. K. Shi, K. Wang, X. Liu, A. Harzheim, A. Lucas, S. Sachdev, P. Kim, T. Taniguchi, K. Watanabe *et al.*, Observation of the Dirac fluid and the breakdown of the Wiedemann-Franz law in graphene, Science **351**, 1058 (2016).
[41] R. Sano and M. Matsuo, Breaking down the magnonic Wiedemann-Franz law in the hydrodynamic regime, Phys. Rev. Lett. **130**, 166201 (2023).
[42] W. O. Wang, J. K. Ding, Y. Schattner, E. W. Huang, B. Moritz, and T. P. Devereaux, The Wiedemann-Franz law in doped Mott insulators without quasiparticles, Science **382**, 1070 (2023).
[43] M. Baldovin, S. Iubini, R. Livi, and A. Vulpiani, Statistical mechanics of systems with negative temperature, Phys. Rep. **923**, 1 (2021).
[44] A. Marques Muniz, F. Wu, P. Jung, M. Khajavikhan, D. Christodoulides, and U. Peschel, Observation of photon-photon thermodynamic processes under negative optical temperature conditions, Science **379**, 1019 (2023).
[45] K. Baudin, J. Garnier, A. Fusaro, N. Berti, C. Michel, K. Krupa, G. Millot, and A. Picozzi, Observation of light thermalization to negative-temperature Rayleigh-Jeans

equilibrium states in multimode optical fibers, Phys. Rev. Lett. **130**, 063801 (2023).
[46] J. Dunkel and S. Hilbert, Consistent thermostatistics forbids negative absolute temperatures, Nat. Phys. **10**, 67 (2014).
[47] R. H. Swendsen and J.-S. Wang, Gibbs volume entropy is incorrect, Phys. Rev. E **92**, 020103(R) (2015).
[48] N. Agraït, A. L. Yeyati, and J. M. van Ruitenbeek, Quantum properties of atomic-sized conductors, Phys. Rep. **377**, 81 (2003).
[49] S. Krinner, T. Esslinger, and J.-P. Brantut, Two-terminal transport measurements with cold atoms, J. Phys. Condens. Matter **29**, 343003 (2017).
[50] F. Lederer, G. I. Stegeman, D. N. Christodoulides, G. Assanto, M. Segev, and Y. Silberberg, Discrete solitons in optics, Phys. Rep. **463**, 1 (2008).
[51] G. Agrawal, *Applications of Nonlinear Fiber Optics*, Optics and Photonics (Elsevier Science, New York, 2001).
[52] See Supplemental Material, which includes Refs. [53–57], at http://link.aps.org/supplemental/10.1103/PhysRevLett.133.116303 for details on the process of formula derivation and more discussion of numerical calculations.
[53] K. O. Rasmussen, T. Cretegny, P. G. Kevrekidis, and N. Grønbech-Jensen, Statistical mechanics of a discrete nonlinear system, Phys. Rev. Lett. **84**, 3740 (2000).
[54] H. Ren, G. G. Pyrialakos, F. O. Wu, P. S. Jung, N. K. Efremidis, M. Khajavikhan, and D. N. Christodoulides, Nature of optical thermodynamic pressure exerted in highly multimoded nonlinear systems, Phys. Rev. Lett. **131**, 193802 (2023).
[55] H. B. Callen, *Thermodynamics and an Introduction to Thermostatistics* (John Wiley & Sons, New York, 1960).
[56] H. Pourbeyram, P. Sidorenko, F. O. Wu, N. Bender, L. Wright, D. N. Christodoulides, and F. Wise, Direct observations of thermalization to a Rayleigh–Jeans distribution in multimode optical fibres, Nat. Phys. **18**, 685 (2022).
[57] G. P. Agrawal, *Applications of Nonlinear Fiber Optics* (Elsevier Science, Amsterdam, 2010).
[58] F. O. Wu, P. S. Jung, M. Parto, M. Khajavikhan, and D. N. Christodoulides, Entropic thermodynamics of nonlinear photonic chain networks, Commun. Phys. **3**, 216 (2020).
[59] L.-A. Wu and D. Segal, Sufficient conditions for thermal rectification in hybrid quantum structures, Phys. Rev. Lett. **102**, 095503 (2009).
[60] B. Li, L. Wang, and G. Casati, Thermal diode: Rectification of heat flux, Phys. Rev. Lett. **93**, 184301 (2004).
[61] N. Li, J. Ren, L. Wang, G. Zhang, P. Hänggi, and B. Li, Phononics: Manipulating heat flow with electronic analogs and beyond, Rev. Mod. Phys. **84**, 1045 (2012).
[62] S. Palafox, R. Román-Ancheyta, B. Çakmak, and O. E. Müstecaplıoğlu, Heat transport and rectification via quantum statistical and coherence asymmetries, Phys. Rev. E **106**, 054114 (2022).
[63] S. Iubini, S. Lepri, R. Livi, and A. Politi, Off-equilibrium Langevin dynamics of the discrete nonlinear Schrödinger chain, J. Stat. Mech. (2013) P08017.
[64] A. Kurnosov, L. J. Fernández-Alcázar, A. Ramos, B. Shapiro, and T. Kottos, Optical kinetic theory of nonlinear multimode photonic networks, Phys. Rev. Lett. **132**, 193802 (2024).